Numerical study of laminar combined convection heat transfer of Al_2O_3-water nanofluid flow in a heated annular pipe

Mohamed BENKHEDDA[1], Toufik BOUFENDI[2*]

[1]Faculty of Sciences, M'Hamed Bougara University, Boumerdes, Algeria
[1]Energy Physics Laboratory, Faculty of Science, Brothers Mentouri University, Constantine, Algeria

[2]Energy Physics Laboratory, Faculty of Science, Brothers Mentouri University, Constantine, Algeria
[*]Corresponding author: boufendit@yahoo.fr

Abstract - This study concerns the 3D flow field and heat transfer of Al_2O_3-water nanofluid, in an annulus. The external pipe is subjected to a uniform heat flux, while the inner cylinder is adiabatic. By using the nanofluid single phase approach and the finite volume method, the numerical simulation is carried out for a fixed radius ratio and solids concentration while the Reynolds and Grashof numbers are varied. Globally, the results show a qualitative similarity with those obtained with a base fluid alone. As expected, the mixed convection Nusselt number becomes more superior to that of the forced convection when the Grashof number is increased. With a fixed Reynolds number, the temperatures undergo a circumstantial variation under the influence of the Gr number with significant azimuthally variation and for the same concentration, temperatures within the nanofluid are strongly influenced by the Re number.

Keywords: combined convection, nanofluid, annular pipe, single phase model, simulation.

Nomenclature

C_p	specific heat, *J/kgK*
D_h	hydraulic diameter *(=D_o-D_i), m*
D_i	inner diameter, *m*
D_o	outer diameter, *m*
g	gravitational acceleration, $m.s^{-2}$
h	heat transfer coefficient, W/$m^2.K$
Gr	Grashof number,
k	thermal conductivity, W/*m.K*
k_B	Boltzman constant,$(= 1.3807 \times 10^{-23}\ J/K)$
L	length duct, *m*
Nu	local Nusselt number, $\left(= \frac{q_w D_h}{k_{nf}(T_w - T_b)}\right)$
p	pressure, kg/$m.s^2$
p^*	dimensionless pressure, $(= \frac{p}{\rho_{nf} V_0^2})$
Pr	Prandtl number,
q_w	heat flux, *(W/m^2)*
Re	Reynolds number,$(= \frac{\rho_{nf}\, V_0\, D_h}{\mu_{nf}})$
r_i	inner radius, *m*
r_i^*	dimensionless inner radius, $r_i^* = \frac{r_i}{D_h}$
r_o	outer radius, *m*
r_o^*	dimensionless inter radius, $r_o^* = \frac{r_o}{D_h}$
t	time, *s*
t^*	dimensionless time $(= \frac{v_0\, t}{D_h})$
T	temperature, *K*
T^*	dimensionless temperature, $\left(= \frac{T - T_0}{q_w D_h / k_{nf}}\right)$
u	radial velocity, *m/s*
u^*	dimensionless radial velocity, $(= \frac{u}{v_0})$
v	axial velocity , *m/s*
v^*	dimensionless axial velocity, $(= \frac{v}{v_0})$
w	tangential velocity, *m/s*
w^*	dimensionless tangential velocity, $(= \frac{w}{v_0})$
z	axial coordinate, *m*
z^*	dimensionless axial Coordinate, $(= \frac{Z}{D_h})$

Greek symbols

α	thermal diffusivity, $(= \frac{\mu_{nf}}{\rho_{nf}})$ m^2/s
β	volumetric expansion coefficient, K^{-1}
θ	angular coordinate, *rad*
μ	dynamic viscosity, *kg m /s*
ρ	density, *kg/ m^3*
$\emptyset$	nanoparticles volume fraction

Subscripts

s	solid phase
f	base fluid

i inner wall
o outer wall
nf nanofluid
w wall
0 inlet condition

1. Introduction

Nanofluid is the term applied to suspension nanoparticules solids of nanometer size (<100 nm), metallic as Cu, Ag or non-metallic as CuO, TiO_2, Al_2O_3 in the conventional fluids as water, oil or ethylene glycol. The thermal conductivity of conventional fluids is very low compared to the solid particles. Then, adds the solid nanoparticles in the fluid to increase the effective thermal conductivity of the mixture. Nanofluids have novel properties that make then potentially useful in many applications, [1, 2]. Masuda et al. [3] worked on the thermal conductivity and the viscosity with suspensions of nanoparticles of Al_2O_3, SiO_2, and TiO_2 , they observed almost 30% increase in the thermal conductivity of nanofluid in comparison with base fluid.

Since a decade ago, researches publications related to the use of nanofluids as active fluids in the mixed convection heat transfer with the fluid flow was retarded numerically and experimentally at the same time. The first work on convective flow and heat transfer of nanofluids, was presented by Pack and Cho [4]. Mixed and forced convection heat transfer in the annular spaces is a significant phenomenon in engineering systems as it is an ordinary and essential geometry for fluid flow and heat transfer devices. This annular geometry has many applications in engineering such as the double pipe exchangers [5], cooling the center of the nuclear reactors, thermal storage systems, solar energy systems, boilers, cooling electronics, thermal isolation, and air conditioning system. Izadi et al. [6] studied forced convection in an annular horizontal pipe numerically they showed that the dimensionless axial velocity remarkable change with the volume concentration but the profile of temperature changes slightly. Mokhtari et al. [7] also studied mixed convection in an annular space and showed the effects of some important parameters such as nanoparticle volume fraction, aspect ratio, Grashof number, and heat flux, it is observed that the local Nusselt number increases with increase in nanoparticle concentration, Grashof number, and radius ratio. Dawood et al. [8] presented reviews of various researches on fluid flow and heat transfer behavior in an annulus. A basic description of the convection heat transfer is given. Numerical and experimental investigations are conducted according to the concentric and eccentric annuli.

At the end of this literature review, it is clear that the convective transfer in a nanofluid deserves some interest in its development in an annular geometry. It is essentially the subject of this article. It is to treat the laminar convective flow of Al_2O_3-water nanofluid in horizontal annuli with constant heat flux imposed at the external cylinder while the internal cylinder is adiabatic and to deduce the influence of different control parameters such as Reynolds and Grashof numbers and the volume concentration solid particles.

2. Thermo-physical Properties of Nanofluid

The physical and thermal properties such as density, viscosity, specific heat, and thermal conductivity of the nanofluids are calculated using different appropriate formulae which are as follows:

The density of the nanofluids is calculated according to Pack and Cho's equation [4]:

$$\rho_{nf} = (1 - \emptyset)\rho_f + \varphi\rho_s \quad (1)$$

The formula for calculating the specific heat of nanofluids. Xuan et al. [2] is:

$$(\rho Cp)_{nf} = (1 - \varphi)(\rho Cp)_f + \varphi(\rho Cp)_s \quad (2)$$

The Hamilton-Crosser [9] model, which introduces the shape factor of the nano particles:

$$k_{nf} = \frac{(k_s+(n-1)k_f)-(n-1)\varphi(k_f-k_s)}{k_s+(n-1)k_f+\varphi(k_f-k_s)} k_f \quad (3)$$

where n is a shape factor defined by $n = 3/\Psi$ and Ψ is the ratio of the sphericity defined as the ratio of the surface area of a sphere with volume equal to that of the particle, to the surface area of the particle, n=3 for spherical nanoparticles.

The Brinkman [10] model for spherical nanoparticle

$$\mu_{nf} = \frac{\mu_f}{(1+\emptyset)^{2.5}} \quad (4)$$

Khanafer et al. [11] provides a model which calculates the coefficient of thermal expansion:

$$(\rho\beta)_{nf} = \left[\frac{1}{1+\frac{(1-\emptyset)\rho_f}{\emptyset\rho_s}} \frac{\beta_s}{\beta_f} + \frac{1}{1+\frac{\emptyset}{(1-\emptyset)} \frac{\rho_s}{\rho_f}}\right]\beta_f \quad (5)$$

The physical properties of the base fluid and Al_2O_3 nanoparticules at 293K are presented in Table 1 [12] and Table 2 shows the properties of nanofluid for various volume fractions

Table 1 : Thermophysics properties at 293 K

	β (K^{-1})	k (W m^{-1} K^{-1})	Cp (J kg^{-1} K^{-1})	ρ (kg m^{-3})	μ (Ns m^{-2})
water	$2.1\ 10^{-4}$	0.613	4179	997.1	8.91×10^{-4}
Al_2O_3	$0.85\ 10^{-5}$	40	765	3970	-

Table 2: Variation of thermophysics properties with particle volume fraction for (Al_2O_3-water) nanofluids

Type of fluide	∅%	μ_{nf}(mP.s)	Cp_{nf} (J $kg^{-1}K^{-1}$)	ρ_{nf}(kg m^{-3})	k_{nf}(W $m^{-1}K^{-1}$)	β_{nf} (K^{-1}
Water	0 %	0,891	4179	997,1	0,613	21
Al_2O_3/water	1 %	0,914	4144,86	1026,83	0,631	20,2
Al_2O_3/water	2 %	0,937	4110,72	1056,56	0,649	19,5
Al_2O_3/water	3 %	0,961	4076,58	1086,29	0,667	18,8
Al_2O_3/water	4 %	0,987	4042,44	1116,02	0,686	18,1
Al_2O_3/water	5 %	1,013	4008,3	1145,74	0,705	17,5
Al_2O_3/water	6 %	1,04	3974,16	1175,47	0,725	16,9
Al_2O_3/water	7 %	1,068	3940,02	1205,2	0,745	16,4
Al_2O_3/water	8 %	1,098	3905,88	1234,93	0,765	15,8
Al_2O_3/water	9 %	1,128	3871,74	1264,66	0,786	15,3
Al_2O_3/water	10 %	1,16	3837,6	1294,39	0,807	14,8

3. Mathematical Formulation

The considered problem is a 3D laminar forced and mixed convection of the (Al_2O_3-water) nanofluid flow in horizontal annular duct of length L, formed by two concentric cylinders, inner radius r_i and outer radius r_o. The outer cylinder is subjected to imposed uniform parietal heat flux while the inner cylinder is adiabatic. Figure 2 shows the geometry of the problem. The single-phase model approach is the mathematical model that will be applied to solve this problem with some simplifying hypothesis. The nanofluid is assumed incompressible and Newtonian with negligible viscous dissipation and pressure working. The fluid and solid phases are in thermal equilibrium with the same velocity of movement and the Boussinesq approximation is adopted.

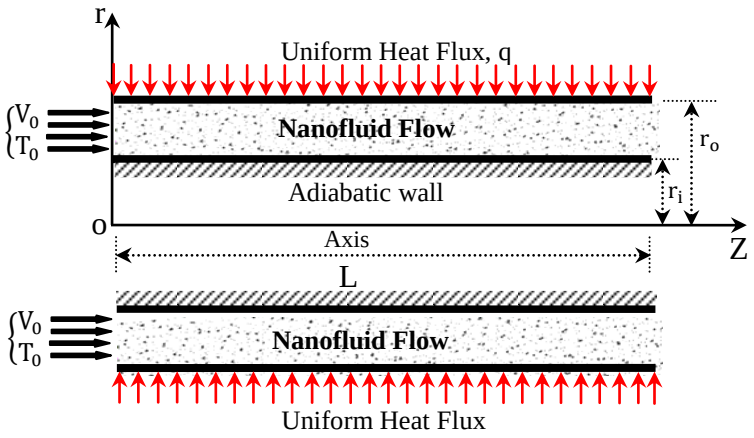

Figure 1: The physical model and the geometry corresponding

a. Governing equation

Under the above mentioned conditions, the conservation equations, written in the dimensionless and vectorial forms with their appropriate boundary conditions are as follows:

At $t^* = 0$:

$$u^* = w^* = v^* = T^* = 0 \tag{6}$$

At $t^* > 0$:

i. Mass equation

$$\frac{\partial \rho}{\partial t^*} + \boldsymbol{\nabla} \cdot (\rho \boldsymbol{V}^*) = 0 \tag{7}$$

ii. Momentum equation

$$\frac{\partial \boldsymbol{V}^*}{\partial t^*} + \boldsymbol{\nabla} \cdot (\boldsymbol{V}^* \boldsymbol{V}^*) = -\boldsymbol{\nabla} P^* + \left[(1/Re_0) \left(\frac{\rho_f}{\rho_{nf}} \frac{1}{(1-\emptyset)^{2.5}} \right) \right] [\boldsymbol{\nabla} \cdot (\mu^* \boldsymbol{\nabla} \boldsymbol{V}^*)] + \left[\left(Gr_0 / Re_0^2 \right) \frac{(1-\emptyset)(\rho\beta)_f + \emptyset(\rho\beta)_s}{\beta_f \times \left((1-\emptyset)\rho_f + \emptyset\rho_s \right)} \right] T^* \tag{8}$$

iii. Energy equation

$$\frac{\partial T^*}{\partial t^*} + \boldsymbol{\nabla} \cdot (\boldsymbol{V}^* T^*) = \left[(1/Re_0 Pr_0) \frac{(\rho C_p)_f}{(\rho C_p)_{nf}} \right] \left[\boldsymbol{\nabla} \cdot \left(\frac{k_{nf}}{k_f} \boldsymbol{\nabla} T^* \right) \right] \tag{9}$$

b. Boundary conditions

This set of nonlinear elliptical governing equations has been solved with the following boundary conditions:

- At the inlet of the duct : ($Z^* = 0$)

$r_i^* \le r^* \le r_o^*$ and $0 \le \theta \le 2\pi$: $u^* = w^* = 0,\ v^* = T^* = 1$ (10)

- At the outlet of the duct : $(Z^* = L^*)$

$$r_i^* \le r^* \le r_o^* ; 0 \le \theta \le 2\pi : \frac{\partial u^*}{\partial Z^*} = \frac{\partial w^*}{\partial Z^*} = \frac{\partial v^*}{\partial Z^*} = \frac{\partial}{\partial Z^*}\left(\frac{\partial T^*}{\partial Z^*}\right) = 0 \quad (11)$$

(the duct length L is 200 time of the hydraulic diameter D_h to insure that the fully developed condition is reached at the outlet)

At the outer wall of the inner cylinder: $r^* = r_i^*$

$$0 \le \theta \le 2\pi,\ 0 \le Z^* \le L^* \qquad u^* = w^* = v^* = 0 \text{ and } \left.\frac{\partial T^*}{\partial r^*}\right|_{r^*=r_i^*} = 0 \quad (12)$$

At the outer wall of the outer cylinder: $r^* = r_o^*$

$$0 \le \theta \le 2\pi,\ 0 \le Z^* \le L^* \qquad u^* = w^* = v^* = 0 \text{ and } \left.\frac{\partial T^*}{\partial r^*}\right|_{r^*=r_o^*} = \frac{k_f}{k_{nf}} \quad (13)$$

Along the angular direction, the periodic conditions are imposed.

The heat transfer is notified by the Nusselt number, which reflects the relative ration of convective to conductive heat transfer. Since the surface of the inner cylinder is adiabatic, the Nusselt number will be reported to the outer surface of the outer cylinder.

At steady state, the local Nusselt number depending on angular and axial position is expressed by the following equation:

$$Nu(\theta, z^*) = \frac{h_o(\theta,z)D}{k_{nf}} = \left[\frac{(k_{nf}/k_f)(\partial T^*/\partial r^*)|_{r^*=1}}{T^*(1,\theta,z^*) - T^*_b(z^*)}\right] \quad (14)$$

where the dimensionless bulk fluid temperature is:

$$T_b^*(z^*) = \frac{\int_{R_i^*}^{R_e^*}\int_0^{2\pi} V^*(r^*,\theta,z^*)T^*(r^*,\theta,z^*)r^* dr^* d\theta}{\int_0^{\frac{1}{2}}\int_0^{2\pi} V^*(r^*,\theta,z^*)r^* dr^* d\theta} \quad (15)$$

The local axial mean peripheral Nu number is:

$$Nu(z^*) = \frac{1}{2\pi}\int_0^{2\pi} Nu(\theta, z^*)d\theta \quad (16)$$

and the average Nu for the whole interface is :

$$Nu(z^*) = \frac{1}{100}\int_0^{100} Nu(z^*)dz^* \quad (17)$$

4. Numerical Resolution

This set of coupled non-linear differential equations was discretized by the finite volume method, Patankar [13]. The temporal discretization of the derivation terms follows the backward Euler scheme whereas the convective and the non-linear terms follow the Adams-Bashfort scheme whose the truncation error is of Δt^{*2}. The spatial disretization of the diffusive terms and the pressure gradient follows the fully implicit central difference scheme. The systems of the linearized algebraic equation obtained are solved by the SIMPLER algorithm, [13]. With step time of $\Delta t^* = 10^{-3}$, the time marching is continued until the steady state is reached. The convergence is confirmed by the satisfaction of the global mass and energy balances. The influence of the mesh has already been the subject of previous work [15]. In the r^*, θ , z^* directions, four numerical grids were used to tests on the influence of the mesh 26x22x42, 26x44x83, 26x44x162 and 26x88x323 successively. It was also verified that the relative difference between the maximum values of the heat flux at the interface does not exceed

0.1% for both high meshes. Finally, so we chose to adopt the 26x44x162 mesh. A validation concerning the forced convection is verified by the comparison of our results with those of Nazrul and al. [14]. The results concern the axial Nusselt number at the interface of the external cylinder and the fluid for the forced convection case. The comparison shows a good agreement, Fig. 2.The numerical code used, is a transformation of the code developed in the first step by Boufendi and Afrid [15] and in the second step by Touahri and Boufendi [16,17].

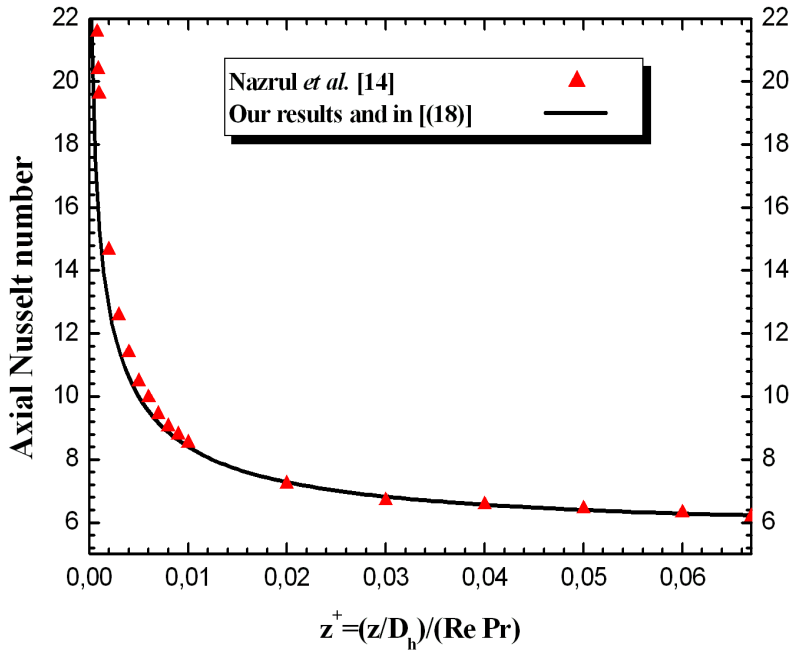

Figure 2: Axial evolution of the mean Nusselt number; comparison with the results of [14]

5. Results and discussion

In this study is presented for different Reynolds number (500 to 2000), and Grashof number 0, 10^4, 10^5, a volume concentration of 4%. The results show:

a. The hydrodynamic and thermal fields

The hydrodynamic (a) and the thermal fields (b) are illustrated in Fig. 4 and 5 for the forced (Gr=0) and mixed cases (Gr=104, 105) at the exit duct. In the forced regime (a), the velocity distribution show a central area where it is high and areas where velocities are low located on either side of this central part.This velocity distribution obeys a parabolic velocity profile which is characteristic of a hydrodynamically developed state. In all the cases studied, this profile is quickly reached near the entrance where the axial velocity assumes a maximum value at the center of the annulus which is about 1.476. From topographically viewpoint, the iso velocities are concentric circles. Thermal fields are also shown in Fig. 4 and 5 for the two cases (b). The topography of the thermal fields shows for the case Fig. 4(b) that the isothermal surfaces are concentric circles whose temperature variation decreases from the outer wall to adiabatic. In all cases the maximum temperatures are on the outer pipe and minimums are on the inner conduit. In the Fig.5 (b), these profiles clearly illustrate the influence of natural convection by the deformation of the isotherms, which are almost flattened in the entire upper part of the annular space. These different qualitative

and quantitative variations are characteristic of the mixed convection in a pipe since the gradients of angular temperatures are not zero. However, two other important points emerge through our results: (i) For the same concentration of nanoparticles, temperatures within the nanofluid are strongly influenced by the Reynolds number. They decrease with increasing Reynolds number. (ii) For the same Reynolds number, temperatures undergo circumstantial change with concentration. They increase substantially with increasing concentration.

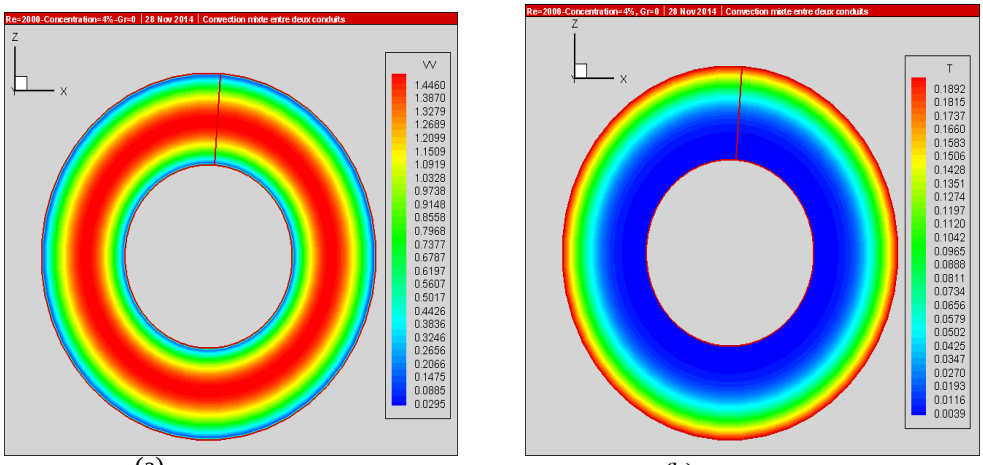

Figure 4: The isolines velocity (a) and the isotherms (b) for Al_2O_3 nanofluid at the exit in forced convection case($Re = 2000, Pr = 6.69;\ \emptyset = 4\%$)

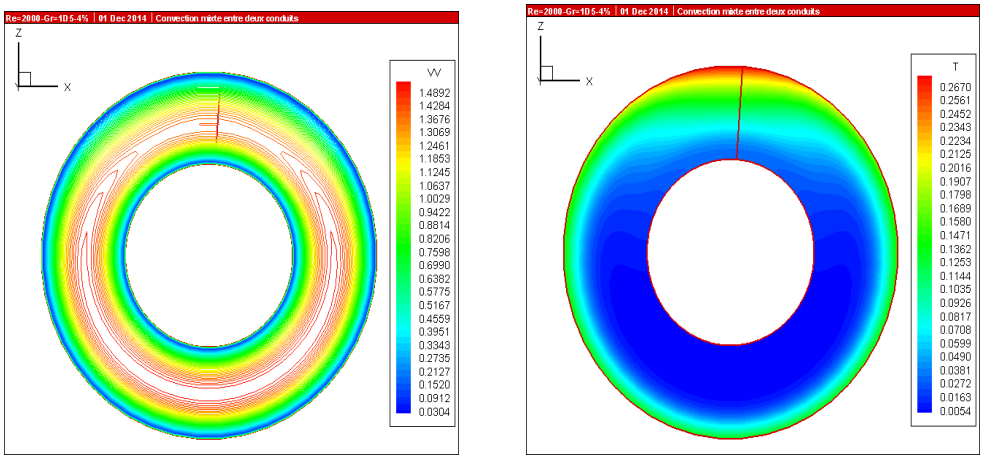

Figure 5: The isoline velocity (a) and the isotherms (b) for Al_2O_3 nanofluid at the exit in mixed convection cases ($Re = 2000, Pr = 6.69;\ \emptyset = 4\%$)

b. Heat transfer

The heat transfer is illustrated with the Nusselt numbers for the forced and mixed convection cases. For the convection mode, Fig. 6 shows the variation of the Nu along the duct for different Reynolds numbers. It is clear that these variations with abrupt decrease in the short entrance zone and a very slow diminution and asymptotic, constant at the large exit zone is physically acceptable with the same behaviour for a fluid flow in forced convection. In contrast, the Fig. 7 illustrates perfectly the effect of the increase of the Grashof number on the evolution of the nanofluid along the pipe. For a same Reynolds number and a same concentration of nanoparticles the Nusselt number increase with the increasing of the Grashof number.

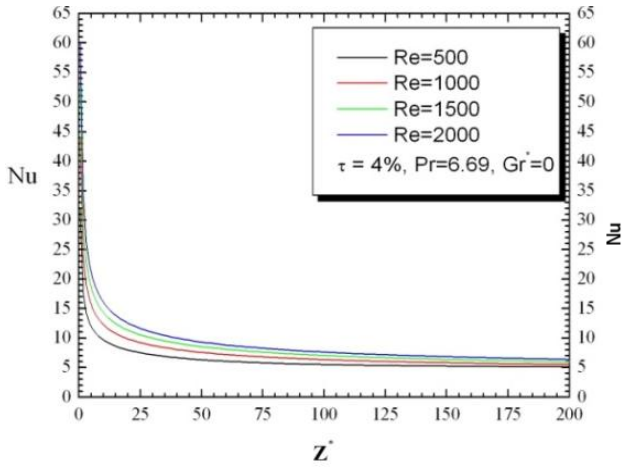

Figure 6: The Nusselt number Profiles along the annulus for the forced convection case

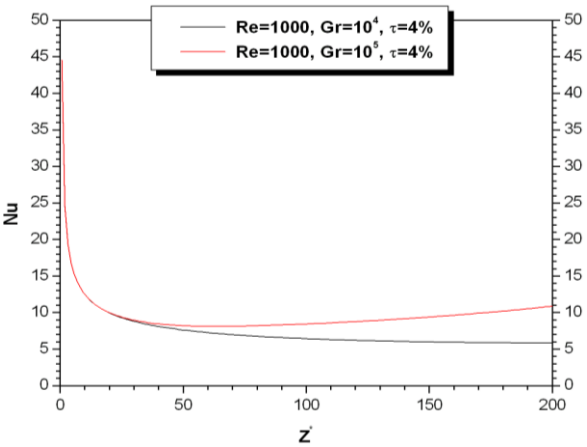

Figure 7: The Nusselt number Profiles along the annulus for the mixed convection case

6. Conclusion

This work is a numerical simulation of convective heat transfer in nanofluid flowing through an annulus formed by two horizontal concentric cylinders. The inner cylinder is adiabatic while the outer cylinder is subjected to constant parietal heating. The results can be synthesized as follow: when the concentration is fixed, the temperature within the nanofluid is strongly influenced by the Reynolds number. They decrease with increasing Reynolds number. Whereas for the same Reynolds number, temperatures undergo circumstantial change with concentration. Also, by the influence of the Grashof number, it is seen that very near the inlet, the variation of the temperature of the interface is similar to that of the forced convection. Under the effect of natural convection, the azimuthally variation of the temperature at the interface becomes large. The increase Grashof increases the heat transfer quantified by growth Nusselt number.

References

90. J. A. Eastman, S. Choi, W. Li, S. Yu, L.J. Thompson. Anomalously increased effective thermal conductivities of ethylene glycol-based nanofluids containing copper nanoparticles. J. Appl. Phys. Letters. 78 (2001) 718–720.

91. Y. Xuan, Q. Li Heat transfer enhancement of nanofluids. Int. J. Heat Fluid Flow. 21 (2000) 58–64.

92. H. Masuda, A. Ebata, K. Teramae, N. Hishinuma, Alteration of thermal conductivity and viscosity of liquid by dispersing ultra-fine particles (dispersion of r-Al2O3, SiO2, and TiO2 ultra-fine particles), Netsu Bussei. Japan, 4 (1993) 227–233.

93. B. Pak, Y.I. Cho. Hydrodynamic and heat transfer study of dispersed fluids with submicron metallic oxide particle. Heat Transfer, 11 (1998) 151–70.

94. H. A. Mohammed. Laminar mixed convection heat transfer in a vertical circular tube under buoyancy-assisted and opposed flows. Ener. Conver. Management. 49 (8) (2006) 1–15.

95. M. Izadi, A. Behzadmehr, D. Jalali-Vahida, Numerical Study of Developing Laminar Forced Convection of a Nanofluid in an Annulus, Int. J. Thermal Sciences, 48 (2009) 2119–2129.

96. R. M. Moghari, F. Talebi, R. Rafee, M. Shariat, Numerical stydy of pressure Drop and Thermal Charateristics of Al_2O_3-Water Nanofluid Flow in Horizontal Annuli, Heat Transfer Engineering, 36 (2) (2015)166-177

97. H.K. Dawood, H.A. Mohammed, N. Azwadi, C. Sidik, K.M. Munisamy, M.A. Wahid, Forced, natural and mixed-convection heat transfer and fluid flow in annulus: A review, Int. Comm. Heat Mass Transfer, 62 (2015)45–57

98. R. L. Hamilton, O. K. Crosser. Thermal conductivity of heterogeneous two-component system. I & EC Fundamental, 1 (3) (1962) 187–191.

99. H.C. Brinkman, The viscosity of concentrated suspensions and solutions, J. Chem. Phys. 20: (1952) 571-581.

100. K. Khanafer, K. Vafai, M. Lightstone, Buoyancy driven heat transfer enhancement in a two dimensional enclosure utilizing nanofluids, Int. J. Heat Mass Transfer. 46 (2003) 3639–3653.

101. Z. Alloui, P. Vasseur, M. Reggio, Natural convection of nanofluids in a shallow cavity heated from below. Int J Thermal Sciences. 50 (2010) 1–9.

102. S. V. Patankar. Numerical Heat Transfer and Fluid Flow. Hemisphere Publishing Corporation, New York, (1980).

103. I. Nazrul, U.N. Gaitonde, G.K. Sharma, Mixed convection heat transfer in the entrance region of horizontal annuli, Int. J. Heat Mass Transfer, 44 11 (2001) 2107-2120.

104. T. Boufendi, M. Afrid, Three-dimensional conjugate conduction-mixed convection with variable fluid properties in a heated horizontal pipe. Rev. Energ. Renouv, 8 (2005) 1-18.

105. S. Touahri, T. Boufendi, Numerical study of the conjugate heat transfer in a horizontal pipe heated by Joulean effect, Thermal Science, 16 1 (2012) 53-67.

106. S. Touahri, T. Boufendi, Conjugate heat transfer with variables fluid properties in a heated horizontal annulus, Heat Transf. Res. 10.1615/HeatTransRes.2015005019 pages 1019-1038 (2015).

107. S.Touahri, T. Boufendi, In: Dincer, I., Çolpan, C. Ö, Kızılkan, Ö., Acar, C., Hamut, H. S., Ezan M. Özbilen, (eds.), Proc. of the 13th Int. Conf. on Clean Energy, Istanbul, Turkey, (2014), 3183-3190.